

This item is the archived peer-reviewed author-version of:

Plasmonic near-field localization of silver core-shell nanoparticle assemblies via wet chemistry nanogap engineering

Reference:

Asapu Ramesh, Ciocarlan Radu-George, Claes Nathalie, Blommaerts Natan, Minjauw Matthias, Ahmad Tareq, Dendooven Jolien, Cool Pegie, Bals Sara, Denys Siegfried,- Plasmonic near-field localization of silver core-shell nanoparticle assemblies via wet chemistry nanogap engineering
ACS applied materials and interfaces - ISSN 1944-8244 - 9:47(2017), p. 41577-41585
Full text (Publisher's DOI): <https://doi.org/10.1021/ACSAMI.7B13965>
To cite this reference: <https://hdl.handle.net/10067/1472430151162165141>

Plasmonic near-field localization of silver core-shell nanoparticle assemblies via wet chemistry nanogap engineering

Ramesh Asapu^a, Radu-George Ciocarlan^b, Nathalie Claes^c, Natan Blommaerts^a, Matthias Minjauw^d, Tareq Ahmad^d, Jolien Dendooven^d, Pegie Cool^b, Sara Bals^c, Siegfried Denys^a, Christophe Detavernier^d, Silvia Lenaerts^a and Sammy W. Verbruggen^{ae}*

^aDepartment of Bioscience Engineering, Campus Groenenborger, University of Antwerp, Groenenborgerlaan 171, Antwerp 2020, Belgium

^bDepartment of Chemistry, Campus Drie Eiken, University of Antwerp, Antwerp, Belgium

^cDepartment of Physics, Campus Groenenborger, University of Antwerp, Antwerp, Belgium

^dDepartment of Solid State Sciences, Ghent University, Ghent, Belgium.

^eCenter for surface Chemistry and Catalysis, KU Leuven, Leuven, Belgium.

*E-mail: sammy.verbruggen@uantwerp.be

Keywords: surface plasmon resonance, silver, core-shell nanoparticles, SERS, Layer-by-Layer, nanogap, COMSOL Multiphysics®

Abstract

Silver nanoparticles are widely used in the field of plasmonics because of their unique optical properties. The wavelength dependent surface plasmon resonance gives rise to a strongly enhanced electromagnetic field, especially at so-called hot spots located in the nanogap in-between metal nanoparticle assemblies. Therefore, the inter-particle distance is a decisive factor in plasmonic applications such as SERS. In this study, the aim is to engineer this inter-particle distance for silver nanospheres using a convenient wet-chemical approach, and to predict and quantify the corresponding enhancement factor using both theoretical and experimental tools. This was done by building a tunable ultra-thin polymer shell around the nanoparticles using the layer-by-layer method, in which the polymer shell acts as a separating inter-particle spacer layer. Comparison of different theoretical approaches and corroborating the results with SERS analytical experiments using silver and silver-polymer core-shell nanoparticle clusters as SERS substrates was also done. Herewith, an approach is provided to estimate the extent of plasmonic near-field enhancement both in theory as well as experimentally.

Introduction

Noble metal nanoparticle synthesis has generated a significant amount of interest in the last few decades, especially in the plasmonics research domain. This is mainly because of the unique surface plasmon resonance effect of noble metals resulting from their wavelength dependent dielectric properties, that give rise to a strongly enhanced near-electric field localized at the metal-dielectric interface^{1,2}. The intense near-electric fields are the primary reason why plasmonic metal nanoparticles of Ag, Au and Pt etc. find wide application in multiple fields of research in diagnostic and optical applications such as biophotonics³⁻⁶, photocatalysis⁷⁻¹⁵, photovoltaics¹⁶⁻²⁰ and surface

enhanced Raman spectroscopy (SERS)²¹⁻²⁶. Moreover, the scope of application with respect to SERS alone is so vast, of which some of the important domains range from imaging of numerous chemical and biological molecules to single molecule detection²⁷⁻³⁰. The plasmonic design of hot spots is of major importance in SERS³¹⁻³³, as controlling the shape, size and spacing of these noble metal nanoparticles through colloidal self-assembly, sputtering and nanolithographic techniques has boosted the usage of the noble metal nanoparticles in such systems³⁴⁻³⁷. Among the noble metals, which possess these unique dielectric properties, silver nanoparticles are highly preferred in SERS application where the electromagnetic enhancement plays a critical role and is a major contributing factor^{31,35,38,39}. This is because silver has a higher near-field enhancement factor compared to other plasmonic metals and silver is also economically more favorable. However, the main drawback associated with silver nanoparticles is the lack of long-term stability and formation of a diffuse silver oxide layer, which reduces the electromagnetic enhancement and has a detrimental effect on SERS^{40,41}.

As a solution to this problem, a protective layer consisting of metal oxides, carbon and carbon based ligand or capping agents can be built around the particle, creating a core-shell structure with a silver core and a protective shell layer^{35,42-44}. Nevertheless, these methods come with a caveat of shielding the intense electric fields at the near vicinity of nanoparticle since these shells commonly range from a couple of nanometers to almost the size of the core particle itself or even larger. For plasmonic applications such as SERS in which electromagnetic enhancement is crucial, this concentrated near-electric field must be available for adsorbed probe molecules to achieve a strong enhancement in the spectroscopic signal. In our previous work¹², a simple yet versatile method to synthesize Ag@polymer core@shell nanospheres using the Layer-by-Layer (LbL) technique for small sized silver nanospheres (<25nm dia.) was presented, by building an ultrathin polymer

shell. The degree of freedom to control the thickness of the protective polymer shell at sub-nanometer level per layer allowed us to regulate the localized near-electric field available at the surface of the core shell nanoparticle.

In this study, we carry out an analysis of the near field and optical properties of silver-polymer core-shell nanospheres using Mie theory⁴⁵ and Finite Element Methods (FEM), and corroborate the findings with SERS experiments. The Mie analytical solution for core-shell nanospheres or coated spheres (called BHCOAT in FORTRAN code by Bohren and Huffman⁴⁶) was implemented in a MATLAB code developed by Adleman⁴⁷. In another method, Maxwell's electromagnetic differential wave equations are solved discretized in space of the computational domain for 3D models, finite element method (FEM), in COMSOL Multiphysics. The results were compared with experimental spectra and the trend in red shift of the surface plasmon resonance peak is followed. These results provide a good estimate of the effective distance from the nanoparticle surface and the vicinity in which the enhanced near-electric fields are active for silver nanospheres. This is validated by Raman experiments by preparing SERS substrates using silver nanosphere and silver-polymer core-shell nanospheres and rhodamine 6G as the Raman probe dye molecule. Also the ultrathin polymer shell is shown to be insulating, thus inhibiting the charge transfer effect that sometimes comes into play depending on the selectivity of the probe molecule adsorption to the surface of nanoparticles. Therefore, charge transfer as a contributing factor could be ruled out. Consequently, we demonstrate that the loss of signal enhancement in SERS with increasing inter-particle distance is a direct result of decreasing electromagnetic enhancement. This is supported by the theoretical near-field simulations performed in COMSOL Multiphysics. Building on the interesting findings of various researchers who have applied Mie theoretical analysis to study near-field enhancement in their research^{2,34,48-50}, this work extends the analysis with metal@polymer

core-shell nano-assemblies and does not only rely on the analytical solution of Mie theory but also includes comparison with experimental synthesis results, SERS experiments and FEM-based field simulations.

Experimental Methods

1. Synthesis of silver-polymer core-shell nanoparticles

The preparation of silver-polymer core-shell nanoparticles was performed as reported in our previous work¹². In brief, colloidal silver nanoparticles were prepared according to an established procedure by Bastús et al.⁵¹. The particles were subsequently coated with alternate layers of positively and negatively charged polyelectrolytes, using polyelectrolyte solutions of 5 g/L PAH (polyallylamine hydrochloride, MW 17.5 KDa Sigma-Aldrich) and 10 g/L PAA (polyacrylic acid, MW 2 KDa Sigma-Aldrich), respectively. The deposition of one alternate layer each of PAH and PAA is called a bilayer, and this cycle was continued until four bilayers were deposited i.e., $\text{Ag}/(\text{PAH}/\text{PAA})_4$, resulting in an 8 layered polymer shell in total. The aliquots stored after each layer deposition are labelled as Ag_LX, where X represents the layer number; for example aliquots after 4 and 8 layer depositions are labelled as Ag_L4 and Ag_L8 respectively. Whereas bare silver nanoparticles are labelled as Ag_L0.

2. Surface Enhanced Raman Spectroscopy

Rhodamine 6G (Sigma Aldrich, Fluorescence bioreagent) dye was used as the Raman probe molecule for SERS measurements and all the measurements were done using glass substrates. The substrates were cleaned in acidic piranha solution (1:3 by volume of concentrated H_2O_2 : H_2SO_4) followed by thoroughly rinsing in Milli-Q water. The cleaned glass substrates were dried in a nitrogen stream and immersed in a 30% methanolic solution of APTES, (3-

Aminopropyl)triethoxysilane, for at least 12 hours. The substrates were rinsed with methanol and dried in nitrogen stream followed by drying at 100°C for 30 min. These substrates were prepared for SERS measurements by dropcasting a mixture of known concentration of R6G (10 μ L of 10⁻⁴ M) and silver nanospheres or silver-polymer core-shell nanospheres. All the samples were allowed to dry in a desiccator for one full day before measurement. All the samples with bare silver and silver-polymer core-shell nanospheres were adjusted to same concentration by dilution and 1 mL of all the solutions were concentrated to within 40 μ L by centrifugation before addition of the dye solution. With a colloidal concentration of 4x10¹¹ NPs/mL, a rough estimation could be made that around 1500 R6G molecules per nanosphere are present in the concentrated 50 μ L sample drop. A reference neat R6G Raman substrate is prepared by dropcasting 50 μ L of 10⁻² M pure R6G dye solution. Raman spectra were recorded multiple times at different locations for each samples and the calculation of enhancement factors are shown in the Supporting Information section and corresponding Table S1 .

3. Characterization

UV-vis absorption spectra were recorded with a Shimadzu 2501 spectrophotometer. Multiple scans were taken in the wavelength range of 300-700 nm with a resolution of 0.2 nm. An average was taken for three consecutive spectral measurements to accurately locate the SPR peak position. Transmission Electron Microscopy (TEM) measurements were performed using a FEI Tecnai TEM operated at 200 kV. A small drop of the colloidal sample was absorbed for 5 minutes onto a Quantifoil copper grid that was coated with a carbon film (3.19 nm). All the Raman measurements were done using a HORIBA XploRA PLUS Raman microscope under the same conditions. A 532 nm diode-pumped solid-state (DPSS) laser with a power of 25 mW was used for excitation and all the spectra were collected with an accumulation time of 20 s. For the nanoscopic measurements

using conductive atomic force microscopy (C-AFM), dilute colloidal solution of silver-polymer core-shell nanoparticles were dropcasted on a substrate pre-coated with gold, in order to attain monolayer coverage. Substrates were attached to a stainless steel sample plate using conductive carbon tape. The sample was loaded in an Omicron VT XA ultra-high vacuum (UHV) AFM, which operates at a base pressure of 10^{-10} mbar. Durable B-doped full diamond tips (FDT) were used for optimum electrical contact, reproducibility and suitable tip resistance.

Theoretical calculations

1. Mie theory analytical solution

In 1908 Gustav Mie developed a theory to understand the various optical phenomena of scattering, absorption and extinction for small colloidal gold nanoparticles suspended in water⁴⁵. The mathematics behind the theory consists of determination of a series of coefficients to solve for the vector wave equations derived from Maxwell's electromagnetic wave theory and provided the first framework to compute scattering of light by small spherical particles. Over decades of research and innovation, Mie theory is now applied in a much broader field ranging from atmospheric science, metamaterials to engineering of plasmonics and near field optics. Albeit, there is always some amount of assumptions involved, for example with respect to the nanoparticle shape. With a plethora of such simplifications, mathematical conjectures, analysis of pitfalls and potpourri of solutions to Mie theory, Bohren and Huffman compiled a work⁴⁶ in 1983, which is still regarded highly. The crucial step forward was the development of an algorithm which simplifies the calculations and was compiled in FORTRAN code. This code was later implemented in different programs, by many researchers, to such an extent that as of today there are hundreds of open source codes, which help the nascent physicist to solve Mie equations analytically. In this

work, the Mie solution was chosen for coated sphere or core-shell nanosphere, developed as BHCOAT FORTRAN code by Bohren⁴⁶, which was implemented in MATLAB by Adleman⁴⁷ in his doctoral thesis. In brief, the code solves for numerous coefficients and calculates the extinction and absorption coefficients for homogenous sphere after derivation of expressions for scattering and extinction coefficients. For more details on the code and the underlying equations, the reader is referred to the Supporting Information section.

When performing the analytical calculations the dielectric data for silver, taken from literature⁵²⁻⁵⁴, is implemented through a wavelength dependent data function, which is called in the main script. Also, the data for water was taken from Segelstein⁵⁵ with a wavelength dependency instead of using a constant value of 1.33. In case of air as surrounding medium, a constant refractive index of 1 is used, whereas for polymer shell material, a constant value of 1.48 is taken from literature⁵⁶. A cubic spline function is implemented to plot the resulting efficiencies against the wavelength and SPR peak position wavelength is identified.

2. Finite element method

Over the last decade, the evolution of faster computational machines has facilitated the finite element method (FEM) to be highly useful to solve for the differential equations of Maxwell's electromagnetic theory in three dimensions. FEM has the advantage of highly useful application in coupling of fields and physical quantities, and the capability to solve for periodic structures and arbitrary shapes. The models involve differential equations which are solved in a 3D domain and discretized in space using large meshing, which has a minor drawback with respect to computation time and large memory space requirement for complex 3D structures. Although with proper usage

of resources and improvisation of solver algorithms with latest versions of computational programs such as COMSOL Multiphysics, the complexity of 3D models is no longer a concern. In this work we make use of the COMSOL Wave Optics module, in which Maxwell's wave equations are solved with respect to the scattered electric field. More details can be found in the Supporting Information section.

3D models of bare silver nanospheres, silver-polymer core-shell nanospheres with varying polymer shell thickness were built in the wave optics physics in COMSOL Multiphysics (ver. 5.3). A z-axis polarized monochromatic plane wave propagating in the x-axis direction was solved for the scattered field in a wavelength domain study. The above equations were implemented in COMSOL by assigning the formulae to the corresponding variables; please refer to the Supporting Information section for a detailed explanation on modeling. To calculate the extinction and absorption efficiencies, the incident excitation wavelength of the monochromatic plane wave was varied in the range of 300-700 nm. COMSOL has inbuilt wavelength dependent refractive index data in its material database, adapted from Johnson and Christy⁵², and the refractive index data for water is imported as an cubic interpolated data from Segelstein⁵⁵. The incident light wavelength is the same as the as the excitation laser wavelength of Raman microscope used in the experiments i.e. 532 nm.

Results and Discussion

As-synthesized core-shell nanoparticles with a silver core and a polymer shell were characterized by UV-vis spectroscopy after each layer deposition (Figure 1a). The decrease in intensity corresponds to loss of nanoparticles during the multiple cycles of washing and centrifuging. A clear red shift in plasmon peak position upon addition of successive polyelectrolyte

layers can be derived from Figure 1b, which is an indication of the gradual increase in particle size due to an increase in encapsulating polymer shell thickness as more polyelectrolyte layers are deposited.

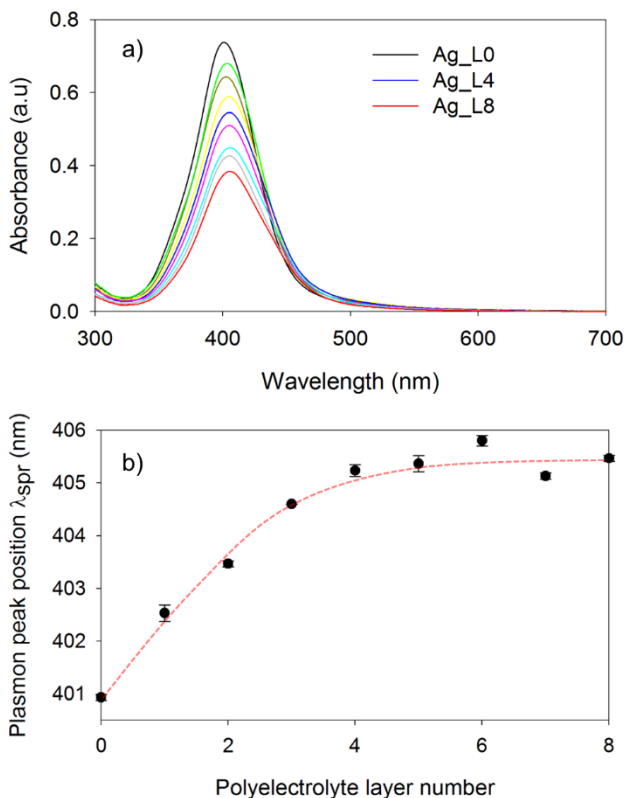


Figure 1. a) UV-vis absorption spectra and b) SPR peak position of silver core-polymer shell nanoparticles as a function of the number of encapsulating layers. The dotted red curve is a trend line of the shift in plasmon peak position.

Also, from bright field transmission electron microscopy (BF-TEM) images in Figure 2, a gradual increase in shell thickness could be observed, with no shell for the bare silver nanoparticles (Figure 2a), and formation of core-shell nanospheres Ag_L4 (Figure 2b and 2c) and Ag_L8 (Figure 2d) encapsulated by a thin shell of thickness 1.7 nm and 2.7 nm, respectively. The TEM images in Figure 2b, 2d represent the pattern in which the core-shell nanoparticles dry on a substrate. Even

though the core-shell nanoparticles seem to be aggregated when dried, the spacing between adjacent particles is controlled by the polymer layer shell thickness. Whereas for bare silver nanoparticles this kind of spacing is not present and the nanoparticles aggregate immediately after the addition into the Raman probe molecule solution.

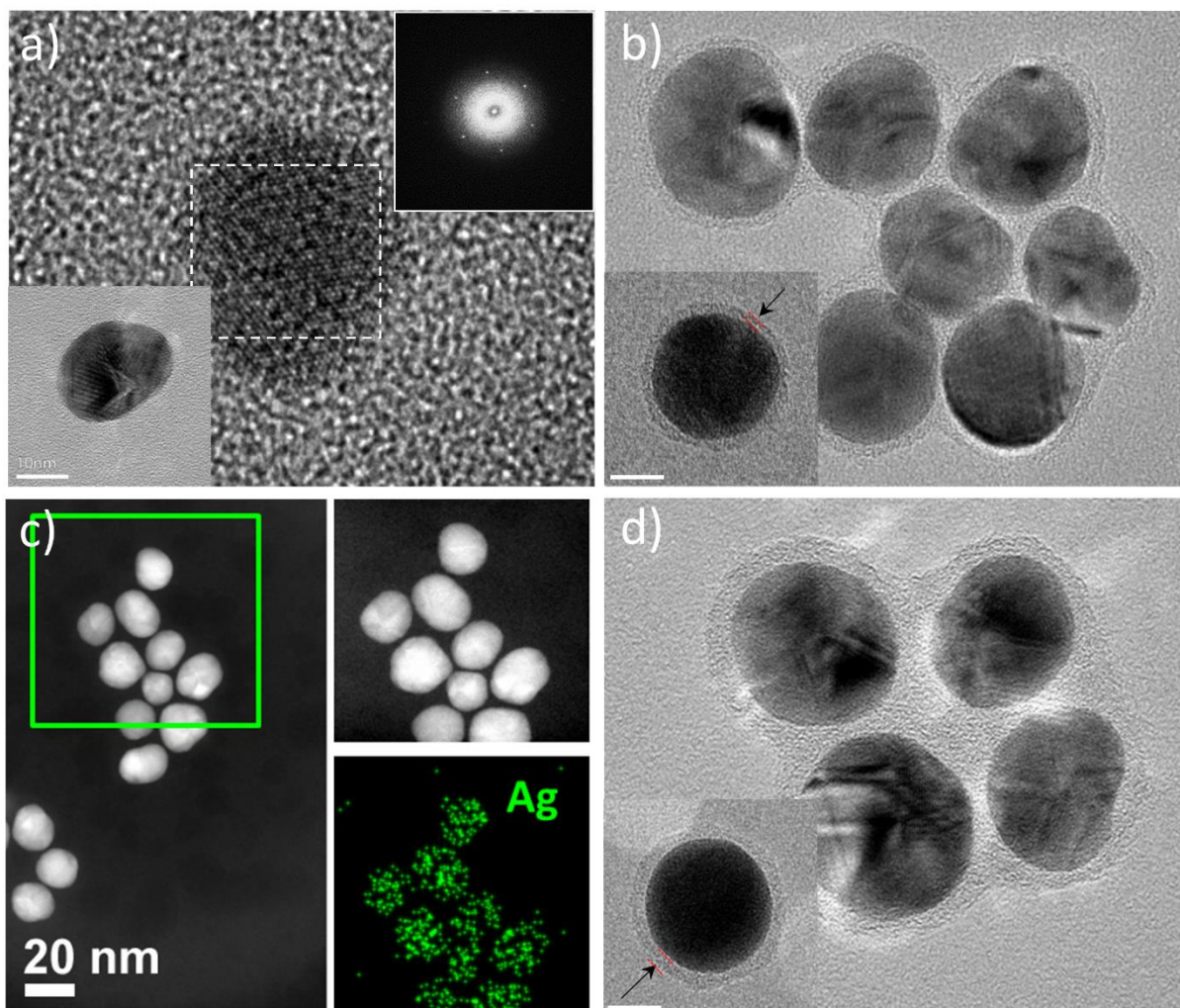


Figure 2. a) HR-TEM image of silver nanoparticle with SAED pattern of silver in the top right corner, b) BF-TEM images of Ag_L4: four layered core-shell nanosphere with a shell thickness of 1.7 ± 0.4 nm, c) HAADF-STEM image of Ag_L4 core-shell nanosphere clusters with EDX map, d) Ag_L8: eight layered core-shell nanosphere with a shell thickness of 2.7 ± 0.6 nm. High resolution

BF-TEM images in the insets are isolated single core-shell nanoparticles with a scale bar corresponding to 10 nm in a, b and d.

The difference in color as seen from Figure S4 for bare and encapsulated silver nanoparticles before and after drying in a desiccator is a clear evidence. The absorbance calculated from Mie analytical MATLAB code and COMSOL was plotted with the experimental absorption spectrum as shown in Figure 3. The optical constants data used for these calculations was taken from literature, and since there are numerous well known datasets, we have primarily used silver permittivity data from Johnson & Christy⁵², Palik⁵³ and Ripken⁵⁴ represented as Mie_J&C, Mie_Palik and Mie_Ripken respectively in the plots for convenience. From the plots, a clear red shift can be observed in all spectra for silver-polymer core shell nanospheres with a shell thickness of 2.7 nm (Ag_L8, Figure 3b) and this for all used datasets.

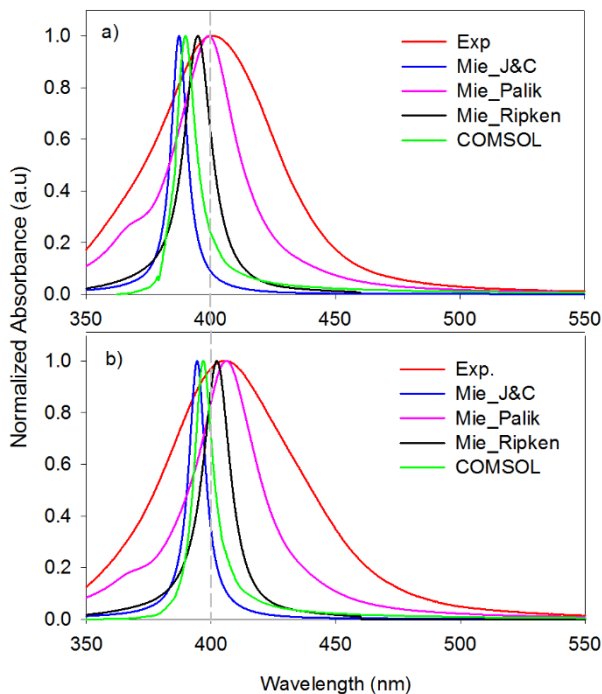


Figure 3. Comparison of normalized UV-vis experimental spectra with calculated theoretical absorption efficiencies for a) bare silver nanospheres and b) silver-polymer core-shell nanospheres with 2.7 nm shell thickness (Ag_L8).

There seems to be a striking difference in the absolute value of the peak position, as well as the shape of the spectrum when using multiple datasets as compared to experimental spectra for both bare Ag nanoparticle and core-shell nanoparticles. This can be attributed to the fact that in Mie analytical calculations and the COMSOL model the nanoparticles are assumed perfectly spherical, of a single size and highly monodisperse, which is rarely the case in a true experimental scenario. The polydispersity of synthesized colloidal nanoparticles is related to the full peak width at half maximum (FWHM) of the spectra, which is not taken into account in Mie calculations nor the COMSOL model. These assumptions will always lead to plasmon band narrowing and a minor shift in the band position for analytical calculations, which is well in line with literature^{34,48,57}. It is also important to note that the datasets used from different researchers vary because the experimental methods used to generate the optical constants are quite different. In addition, each method uses independent corrections in mean free path of electrons for the calculations of the dielectric parameters, in cases where particle sizes get too small. However, the trend in the red shift of plasmon peak position with increased shell thickness is mostly in agreement with the experiments (Figure 4). Still, for a shell thickness of 2.7 nm (Ag_L8), the red shift becomes less substantial than for thinner shells (also clear from the plateau that is reached in Figure 1b). The theoretical calculations on the other hand still show a significant red shift with increase in polymer shell thickness. Such an experimental leveling off of the red shift is expected for core-shell nanoparticles

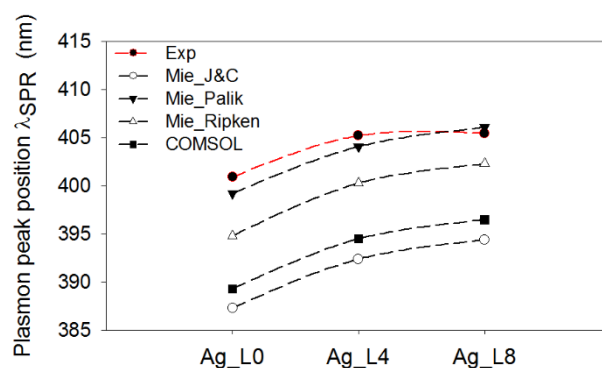


Figure 4. Comparison of experimental spectra with theoretical calculations in water, showing the Plasmon peak position of bare (Ag_L0) and core-shell nanospheres (Ag_L4, Ag_L8).

with thick optically transparent shells, as the shift in the plasmon peak becomes insignificant⁵⁷. It also depends on the refractive index of the surrounding medium, as obviously noticeable from the theoretical equations (Supporting Information). Figure 5 depicts the trend in red shift of the plasmon peak with increasing shell thickness, calculated for air and water as surrounding media. This implies that, as the ratio of the refractive indices of the shell *versus* the surrounding medium becomes closer to unity, the red shift in plasmon peak as a result of increasing shell thickness will slowly disappear. In other words, there would be a blue shift in plasmon peak position if the core-shell nanoparticles were suspended in a medium with a refractive index that is higher than that of shell. Among all the datasets, Mie_Palik seems to match best with the experimental red shift (Figure 4). For the experimental dataset a plateau value is reached, which is not yet the case for the theoretical calculations in this range of shell thickness. This deviation can potentially be attributed to the use of a constant refractive index for a composite of polyelectrolyte layers in the calculations. From a practical point of view small deviations in shell thickness or imperfections within the polymer composite are also possible. Overall, it should be clear that the shell thickness

is a crucial factor for plasmonic core-shell nanoparticles as it has a significant effect on both optical as well as near-field properties.

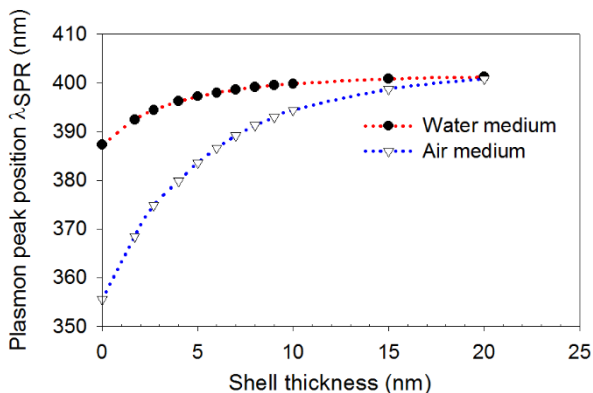


Figure 5. Mie analytical calculations showing the red shift in plasmon peak position as a function of increasing polymer shell thickness for core-shell nanospheres in air and water as the surrounding medium.

As discussed earlier, for plasmonic nanomaterials like silver nanospheres, enhanced near-fields are the main asset for plasmonic applications such as SERS. Therefore, it is important to study how the shell affects these near-field properties. In addition, another main scope of this work is to find out the distance or vicinity from the surface of the nanosphere to which the enhanced near-field is confined. For this specific purpose, SERS is used as an experimental tool to verify the resulting plasmonic enhancement when applying polymer shells of varying thicknesses as an interface building material to adjust the near field localization of silver nanospheres. In other words, by building polymer shells with high control over the resulting thickness, the nanogap between two adjacent silver cores can be tuned and the resulting hot spot effect can be regulated. As explained in the experimental section, SERS substrates are prepared using bare silver nanospheres (Ag_L0) and silver-polymer core-shell nanospheres with two different shell thicknesses (Ag_L4, Ag_L8).

Figure 6a shows the SERS measurements of different substrates, and significant enhancements are found for 10^{-4} M R6G in the presence of both bare silver nanospheres (Ag_L0) and silver-polymer core-shell nanospheres with a shell thickness of 1.7 nm (Ag_L4). The Raman intensity for the neat R6G substrate of 0.01 M R6G is amplified five times for better visualization in the common intensity scale. However, little to no enhancement/signal could be detected for R6G in presence of core-shell nanoparticle with a shell thickness of 2.7 nm (Ag_L8). The decrease in the experimental SERS enhancement factors (EFs) calculated from the Raman measurements are shown in Figure 6b. The EFs are calculated by using the integrated intensity of the 1365 cm^{-1} band of the C-C/C-N stretch of the R6G molecule at which major enhancement in signal is recorded. From the measurements, it can be inferred that significantly high enhancement ($\text{EF} \sim 1.2 \times 10^4$) is shown by bare silver nanospheres; and a considerable decline in EF ($\sim 1.8 \times 10^3$) is observed when the Ag nanospheres coated with a shell thickness of 1.7 nm are used. Also, when the silver nanoparticles are coated with a shell of thickness 2.7 nm or more, insignificant experimental enhancement of the Raman signal could be achieved.

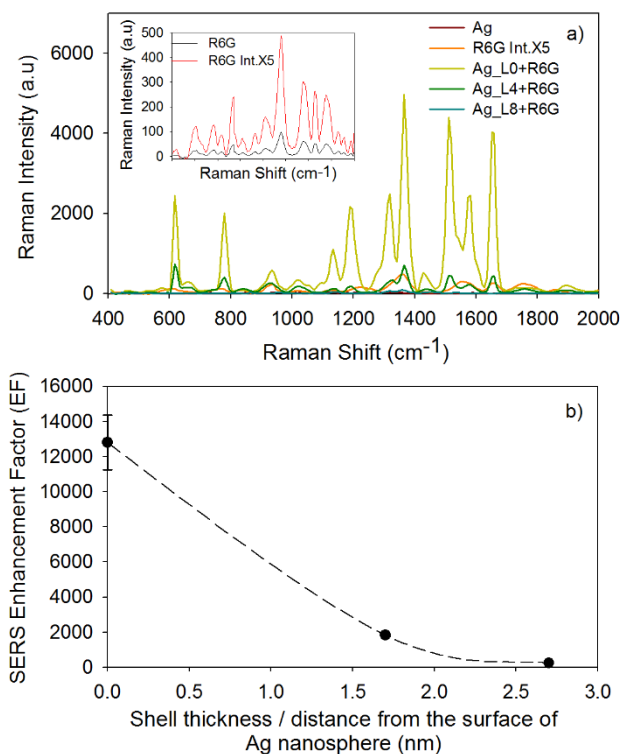


Figure 6. a) SERS measurements of pure Ag nanospheres, 10 mM R6G (intensity amplified 5 times, original and amplified spectra shown in inset), and 0.1 mM R6G with substrates of Ag nanospheres, Ag_L4 and AgL8 core-shell nanospheres; b) SERS enhancement factor as a function of distance from the silver nanosphere surface.

This indicates that the shell thickness i.e., the distance from the surface of the Ag nanoparticles plays a major role in regulating the enhanced near-electric fields available at the surface of the nanoparticle. In other words tuning the distance between the Raman probe molecules and the surface of the Ag nanospheres is achieved by controlling the thickness of polyelectrolyte layers. Therefore, investigating the effect of shell thickness on the near-field enhancement through field simulations using FEM, will be very helpful. In this work, COMSOL Multiphysics was used to perform the near field simulations using FEM and the results are shown in Figure 7. The experimental SERS EM enhancement can be a result of near-field generated by either a single

nanosphere, or from the hot spots created in-between the nanogap of nanoparticle assemblies. Analyzing the field simulation maps in Figure 7a and the quantified theoretical EFs (using the $|E/E_0|^4$ estimation²⁵, see

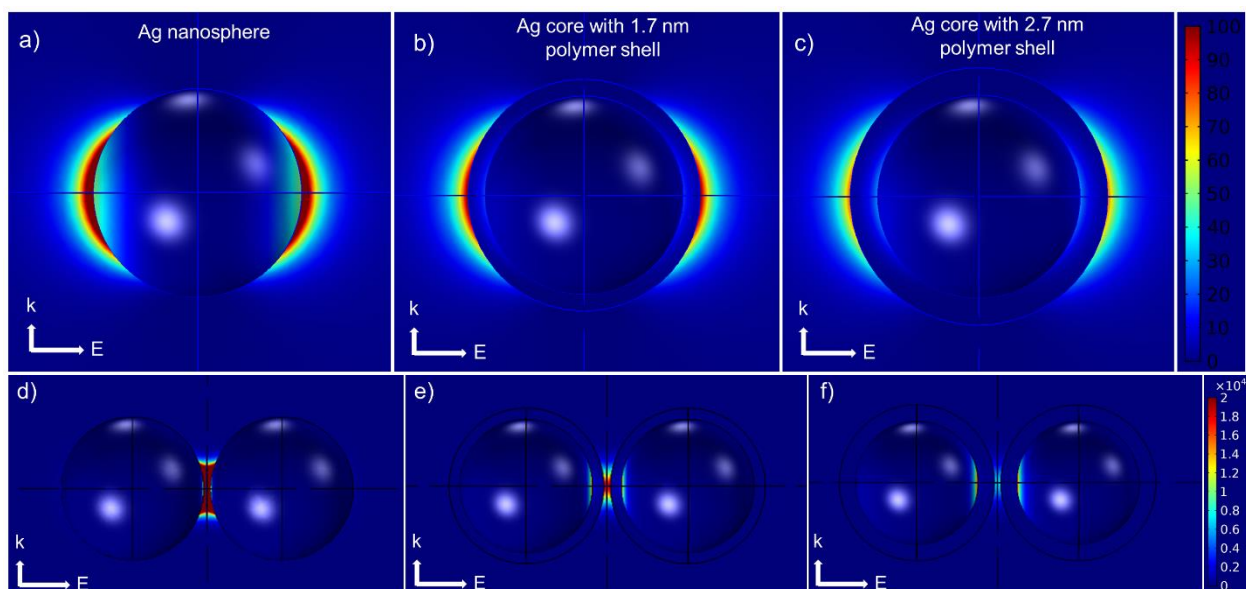


Figure 7. a) Near-field simulation maps at the Raman excitation wavelength of 532 nm in air for a) Ag nanosphere and Ag-polymer core-shell nanosphere with a shell thickness of b) 1.7 nm (Ag_L4) and c) 2.7 nm (Ag_L8), and the corresponding dimers of the nanospheres d), e), f). The scale ($|E/E_0|^4$) is normalized at 100 for single nanospheres and 2×10^4 for dimers respectively for better visualization of the enhanced fields.

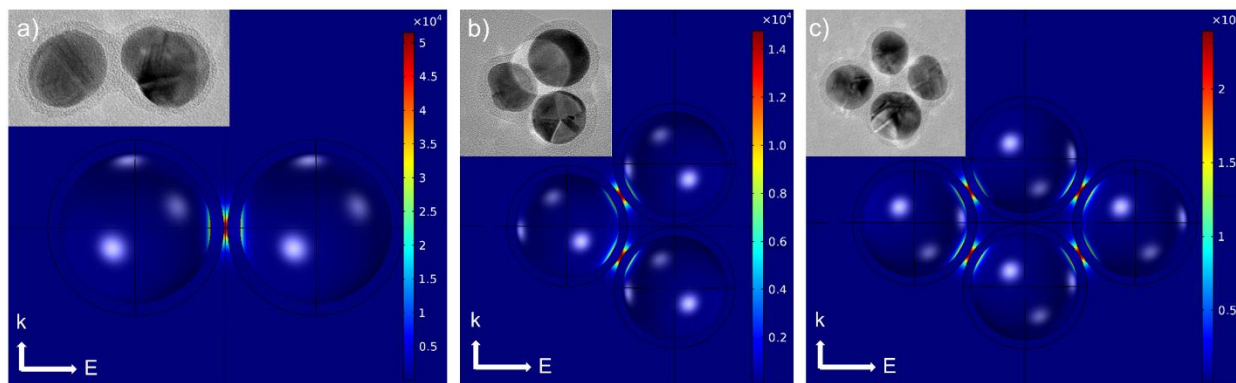


Figure 8. Field enhancement maps for a) dimer b) trimer and c) tetramer silver-polymer core-shell nanoparticle clusters with TEM inset images for representation. The colour legends are in the scale of $|E/E_0|^4$ representing the magnitude of maximum theoretical SERS EF.

Supporting Information Figure S3), the maximum EF is found to be only in the order of 10^2 for single Ag nanosphere and drops significantly with increase of shell thickness. Such low theoretical EFs do not match the high experimentally observed EF. So, the high EFs achieved from SERS experiments can only be explained by a major contribution from the intense near-fields produced in the hot spots^{30,31,58} i.e., the nanogaps between nanoparticles. It can be assumed that the hot spot in the nanosphere dimer is of the same order of magnitude as in nanoparticle clusters with the exception of formation of high spatial localization in 3D structures. This assumption is mainly for ease of visualization and analysis of hot spots in field simulation maps. In addition, the magnitude of the near field in nanogaps of dimers, trimers or tetramers is not significantly different as evidenced by theoretical simulations (Figure 8). The field enhancement maps for the dimer systems, with a nanogap of 1 nm, are shown in Figure 7b and one can observe that the hot spot intensity decreases for a shell thickness of 1.7 nm, and becomes almost non-existent for shell thickness of 2.7 nm. This is in good agreement with the experimental observation of the SERS EFs which is also observed from Figure 9 which shows a comparison between theoretical and

experimental SERS EF. Moreover, there is a very good match for the decay ratio of SERS EF with increasing shell thickness. To estimate the theoretical enhancement factor from simulations, a nanogap of 2 nm between two nanoparticles is considered to match the condition when one each R6G dye molecule are adsorbed on the adjacent particles providing a spacing layer.

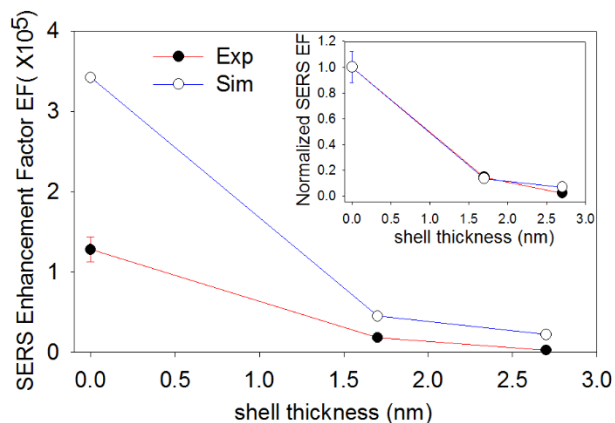


Figure 9. Comparison of theoretical and experimental SERS enhancement factors. Inset shows the comparison with a normalized enhancement factor.

Eventually these analyses provide a more realistic picture that beyond a distance/vicinity of 1.7 nm from the surface of nanoparticle the EM enhancement becomes negligible. These results are in line with the literature^{26,40,59}, where it has been reported that within 1-2 nanometer from the surface of plasmonic nanoparticle, the enhancement is radically reduced. There is a possibility that an ultrathin polymer layer of 1.7 nm may be inherently enhancing the Raman signal through chemical enhancement when the adsorbed R6G molecule interacting with the polymer chain allows for a quick charge transfer. To investigate this potential contribution, conductive tip atomic force microscopy (C-AFM) measurements were performed to find the charge transfer properties of silver-polymer core-shell nanoparticles. The reason for using C-AFM to determine the electrical properties of the core-shell nanoparticles is that the polymer blends have unique electrical properties depending on the type of polymers used. Merely measuring the current-voltage (IV)

properties of the as-prepared silver-polymer core-shell nanocluster film can lead to false interpretations when using a typical four-point probe method to determine the resistivity. This is because in a dried nanocluster film the polymer shells of adjacent nanoparticles are in contact and the resulting resistance is in fact that of a long nanoparticle chain. So, a more robust methodology is adapted by immersing a gold coated Si wafer in a dilute colloidal solution of silver-polymer core-shell nanoparticles to make sure single isolated core-shell nanoparticles could be imaged by AFM. This is followed by applying a voltage through the conductive cantilever tip of the AFM and the detected current levels indicate the resistance of the core-shell nanoparticle on the gold substrate. From Figure 10, it can be observed that a core-shell nanoparticle with a shell thickness of 1.7 nm is highly insulating and resists charge transfer. Both particles in the AFM surface image showed no passage of current with increase in voltage until the AFM cantilever tip tunneled through the particle and made contact with the gold substrate underneath. This is a classic tunneling IV profile for high resistance or insulating materials. This measurement rules out chemical enhancement due to charge transfer through the ultrathin polymer shell. This also supports the fundamental theory that near-field or EM enhancement is the major mechanism responsible for SERS as established in the literature^{21–23,60}.

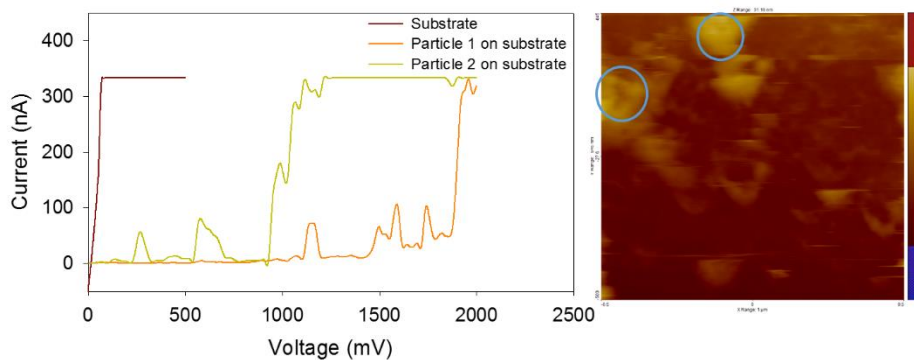


Figure 10. Conductive tip AFM measurements performed on gold substrate and on two core-shell nanospheres deposited on substrate, the surface image shows the location of two particles.

As a final remark it should be noted that due to the size- and shape dependence of SPR on metal nanoparticles like silver, this can and will affect the hot spots and correlated intensity enhancement that can be achieved in SERS. Additionally, using different polymer materials for the shell (either insulating or conductive) will also have an impact as long as there is a significant change in the refractive index of the polymer materials used. Nonetheless, the replication of the LbL procedure and resulting parameters of shell thickness and corresponding red-shifts confirm excellent repeatability (Supporting Information Figure S5). The findings presented in this study based on an average silver nanoparticle size of 20 nm and its corresponding polymer combinations to tune the nanogap in-between, should therefore be regarded as a more generic approach to fine-tune the near-field localization of plasmonic nanoparticles for various other core-shell composite nanostructures.

Conclusion

This study demonstrates how experimental methods in conjunction with theoretical simulations can act as a vital mechanistic tool to understand the plasmonic properties of silver nanoparticles. In this way the effect of shell thickness on the optical properties of core-shell nanoparticles and nanoparticle assemblies is thoroughly examined. The application of a spacer layer through wet chemical methods such as LbL can be used to effectively engineer the size of the nanogap in-between adjacent particles. This is important, as it is shown that the distance from the particle core greatly affects the near-field and resulting SERS enhancement. Comparison with theoretical FEM field simulations indicates that experimentally obtained enhancement factors in SERS are mainly determined by the enhanced near electric field generated at the hot spot zones in-between particles, of which the nanogap can be regulated through the thickness of the spacer shell layer. These tools and insights will aid in more straightforward nano-engineering of substrates for plasmonic

applications to target the localized vicinity of field enhancement and make use of hot spot effects of such plasmonic nanoparticles. Moreover, it will help identify and engineer the optimal inter-particle distance, customized to a particular plasmonic application.

AUTHOR INFORMATION

Corresponding Author

*Prof. dr. ir. Sammy W. Verbruggen. Sammy.verbruggen@uantwerpen.be

Author Contributions

The manuscript was written through contributions of all authors. All authors have given approval to the final version of the manuscript.

ACKNOWLEDGEMENTS

M. Minjauw, J. Dendooven and S.W. Verbruggen acknowledge FWO Vlaanderen for financial support through a research fellowship. C. Detavernier wishes to thank the Hercules foundation for financial support (SPINAL). P. Cool and R-G. Ciocarlan acknowledge financial support by FWO Vlaanderen (project nr. G038215N). N. Claes and S. Bals acknowledge financial support from European Research Council (ERC Starting Grant #335078-COLOURATOM).

References

- (1) Murray, W. A.; Barnes, W. L. Plasmonic Materials. *Adv. Mater.* 2007, *19* (22), 3771–3782.
- (2) Hutter, T.; Huang, F. M.; Elliott, S. R.; Mahajan, S. Near-Field Plasmonics of an Individual Dielectric Nanoparticle above a Metallic Substrate. *J. Phys. Chem. C* 2013, *117* (15), 7784–7790.
- (3) West, J. L.; Halas, N. J. Engineered Nanomaterials for Biophotonics Applications: Improving Sensing, Imaging, and Therapeutics. *Annu. Rev. Biomed. Eng.* 2003, *5* (1), 285–292.
- (4) Haes, A. J.; Haynes, C. L.; McFarland, A. D.; Schatz, G. C.; Van Duyne, R. P.; Zou, S. Plasmonic Materials for Surface-Enhanced Sensing and Spectroscopy. *MRS Bull.* 2005, *30* (5), 368–375.
- (5) Khlebtsov, N. G. Optics and Biophotonics of Nanoparticles with a Plasmon Resonance. *Quantum Electron.* 2008, *38* (6), 504–529.
- (6) Willets, K. A.; Van Duyne, R. P. Localized Surface Plasmon Resonance Spectroscopy and Sensing. *Annu. Rev. Phys. Chem.* 2007, *58* (1), 267–297.
- (7) Verbruggen, S. W. TiO₂ Photocatalysis for the Degradation of Pollutants in Gas Phase: From Morphological Design to Plasmonic Enhancement. *J. Photochem. Photobiol. C Photochem. Rev.* 2015, *24*, 64–82.
- (8) Boerigter, C.; Campana, R.; Morabito, M.; Linic, S. Evidence and Implications of Direct Charge Excitation as the Dominant Mechanism in Plasmon-Mediated Photocatalysis. *Nat. Commun.* 2016, *7*, 10545.

- (9) Linic, S.; Christopher, P.; Ingram, D. B. Plasmonic-Metal Nanostructures for Efficient Conversion of Solar to Chemical Energy. *Nat. Mater.* 2011, *10* (12), 911–921.
- (10) Ingram, D. B.; Christopher, P.; Bauer, J. L.; Linic, S. Predictive Model for the Design of Plasmonic Metal/Semiconductor Composite Photocatalysts. *ACS Catal.* 2011, *1* (10), 1441–1447.
- (11) Verbruggen, S. W.; Keulemans, M.; Goris, B.; Blommaerts, N.; Bals, S.; Martens, J. A.; Lenaerts, S. Plasmonic “rainbow” Photocatalyst with Broadband Solar Light Response for Environmental Applications. *Appl. Catal. B Environ.* 2016, *188*, 147–153.
- (12) Asapu, R.; Claes, N.; Bals, S.; Denys, S.; Detavernier, C.; Lenaerts, S.; Verbruggen, S. W. Silver-Polymer Core-Shell Nanoparticles for Ultrastable Plasmon-Enhanced Photocatalysis. *Appl. Catal. B Environ.* 2017, *200*, 31–38.
- (13) Verbruggen, S. W.; Keulemans, M.; Filippousi, M.; Flahaut, D.; Van Tendeloo, G.; Lacombe, S.; Martens, J. a.; Lenaerts, S. Plasmonic Gold-Silver Alloy on TiO₂ Photocatalysts with Tunable Visible Light Activity. *Appl. Catal. B Environ.* 2014, *156–157*, 116–121.
- (14) Blommaerts, N.; Asapu, R.; Claes, N.; Bals, S.; Lenaerts, S.; Verbruggen, S. W. Gas Phase Photocatalytic Spiral Reactor for Fast and Efficient Pollutant Degradation G R a P H I c a L a B S T R a c T. *Chem. Eng. J.* 2017, *316*, 850–856.
- (15) Awazu, K.; Fujimaki, M.; Rockstuhl, C.; Tominaga, J.; Murakami, H.; Ohki, Y.; Yoshida, N.; Watanabe, T. A Plasmonic Photocatalyst Consisting of Silver Nanoparticles Embedded in Titanium Dioxide. *J. Am. Chem. Soc.* 2008, *130* (5), 1676–1680.
- (16) Atwater, H. A.; Polman, A. Plasmonics for Improved Photovoltaic Devices. *Nat. Mater.* 2010, *9* (3), 205–213.

(17) Brown, M. D.; Suteewong, T.; Kumar, R. S. S.; D’Innocenzo, V.; Petrozza, A.; Lee, M. M.; Wiesner, U.; Snaith, H. J. Plasmonic Dye-Sensitized Solar Cells Using Core–Shell Metal–Insulator Nanoparticles. *Nano Lett.* 2011, *11* (2), 438–445.

(18) Sharma, M.; Pudasaini, P. R.; Ruiz-Zepeda, F.; Vinogradova, E.; Ayon, A. A. Plasmonic Effects of Au/Ag Bimetallic Multispiked Nanoparticles for Photovoltaic Applications. *ACS Appl. Mater. Interfaces* 2014, *6* (17), 15472–15479.

(19) Clavero, C. Plasmon-Induced Hot-Electron Generation at Nanoparticle/metal-Oxide Interfaces for Photovoltaic and Photocatalytic Devices. *Nat. Photonics* 2014, *8* (2), 95–103.

(20) Sandén, S.; Akitsu, K.; Törngren, B.; Ylinen, A.; Smått, J. H.; Kubo, T.; Matsumura, M.; Otani, N.; Segawa, H.; Österbacka, R. Plasmon-Enhanced Polymer-Sensitized Solar Cells. *J. Phys. Chem. C* 2015, *119* (10), 5570–5576.

(21) Sharma, B.; Frontiera, R. R.; Henry, A.-I.; Ringe, E.; Van Duyne, R. P. SERS: Materials, Applications, and the Future. *Mater. Today* 2012, *15* (1–2), 16–25.

(22) Schlücker, S. Surface-Enhanced Raman Spectroscopy: Concepts and Chemical Applications. *Angew. Chemie - Int. Ed.* 2014, *53* (19), 4756–4795.

(23) McFarland, A. D.; Young, M. A.; Dieringer, J. A.; Van Duyne, R. P. Wavelength-Scanned Surface-Enhanced Raman Excitation Spectroscopy. *J. Phys. Chem. B* 2005, *109* (22), 11279–11285.

(24) Leopold, N.; Lendl, B. A New Method for Fast Preparation of Highly Surface-Enhanced Raman Scattering (SERS) Active Silver Colloids at Room Temperature by Reduction of Silver Nitrate with Hydroxylamine Hydrochloride. *J. Phys. Chem. B* 2003, *107* (24), 5723–5727.

(25) Stiles, P. L.; Dieringer, J. A.; Shah, N. C.; Van Duyne, R. P. Surface-Enhanced Raman Spectroscopy. *Annu. Rev. Anal. Chem.* 2008, *1* (1), 601–626.

(26) Dieringer, J. A.; McFarland, A. D.; Shah, N. C.; Stuart, D. A.; Whitney, A. V; Yonzon, C. R.; Young, M. A.; Zhang, X.; Van Duyne, R. P. Surface Enhanced Raman Spectroscopy: New Materials, Concepts, Characterization Tools, and Applications. *Faraday Discuss.* 2006, *132*, 9–26.

(27) Lim, D.-K.; Jeon, K.-S.; Kim, H. M.; Nam, J.-M.; Suh, Y. D. Nanogap-Engineerable Raman-Active Nanodumbbells for Single-Molecule Detection. *Nat. Mater.* 2010, *9* (1), 60–67.

(28) Radziuk, D.; Moehwald, H. Prospects for Plasmonic Hot Spots in Single Molecule SERS towards the Chemical Imaging of Live Cells. *Phys. Chem. Chem. Phys.* 2015, *17* (33), 21072–21093.

(29) Liu, R.; Liu, B.; Guan, G.; Jiang, C.; Zhang, Z. Multilayered Shell SERS Nanotags with a Highly Uniform Single-Particle Raman Readout for Ultrasensitive Immunoassays. *Chem. Commun. (Camb)*. 2012, *48* (75), 9421–9423.

(30) Blackie, E. J.; Ru, E. C. Le; Etchegoin, P. G. Single-Molecule Surface-Enhanced Raman Spectroscopy of Nonresonant Molecules. *J. Am. Chem. Soc.* 2009, *131* (40), 14466–14472.

(31) Xu, H.; Aizpurua, J.; Käll, M.; Apell, P. Electromagnetic Contributions to Single-Molecule Sensitivity in Surface-Enhanced Raman Scattering. *Phys. Rev. E - Stat. Physics, Plasmas, Fluids, Relat. Interdiscip. Top.* 2000, *62* (3 B), 4318–4324.

(32) Kleinman, S. L.; Frontiera, R. R.; Henry, A.-I.; Dieringer, J. a; Van Duyne, R. P. Creating, Characterizing, and Controlling Chemistry with SERS Hot Spots. *Phys. Chem. Chem. Phys.* 2013, *15* (1), 21–36.

(33) Li, W.; Camargo, P. H. C.; Lu, X.; Xia, Y. Dimers of Silver Nanospheres: Facile Synthesis and Their Use as Hot Spots for Surface-Enhanced Raman Scattering. *Nano Lett.* 2009, *9* (1), 485–490.

(34) Kelly, K. L.; Coronado, E.; Zhao, L. L.; Schatz, G. C. The Optical Properties of Metal Nanoparticles: The Influence of Size, Shape, and Dielectric Environment. *J. Phys. Chem. B* 2003, *107* (3), 668–677.

(35) Radziuk, D.; Möhwald, H. Surpassingly Competitive Electromagnetic Field Enhancement at the Silica/silver Interface for Selective Intracellular Surface Enhanced Raman Scattering Detection. *ACS Nano* 2015, *9* (3), 2820–2835.

(36) Chan, G. H.; Zhao, J.; Hicks, E. M.; Schatz, G. C.; Van Duyne, R. P. Plasmonic Properties of Copper Nanoparticles Fabricated by Nanosphere Lithography. *Nano Lett.* 2007, *7* (7), 1947–1952.

(37) Stamplecoskie, K. G.; Scaiano, J. C.; Tiwari, V. S.; Anis, H. Optimal Size of Silver Nanoparticles for Surface-Enhanced Raman Spectroscopy. *J. Phys. Chem. C* 2011, *115* (5), 1403–1409.

(38) Gill, R.; Tian, L. J.; Somerville, W. R. C.; Le Ru, E. C.; van Amerongen, H.; Subramaniam, V. Silver Nanoparticle Aggregates as Highly Efficient Plasmonic Antennas for Fluorescence Enhancement. *J. Phys. Chem. C* 2012, *116* (31), 16687–16693.

(39) White, P.; Hjortkjaer, J. Preparation and Characterisation of a Stable Silver Colloid for SER(R)S Spectroscopy. *J. Raman Spectrosc.* 2014, *45* (1), 32–40.

(40) Han, Y.; Lupitsky, R.; Chou, T. M.; Stafford, C. M.; Du, H.; Sukhishvili, S. Effect of Oxidation on Surface-Enhanced Raman Scattering Activity of Silver Nanoparticles: A Quantitative Correlation. *Anal. Chem.* 2011, *83* (15), 5873–5880.

(41) Erol, M.; Han, Y.; Stanley, S. K.; Stafford, C. M.; Du, H.; Sukhishvili, S. SERS Not To Be Taken for Granted in the Presence of Oxygen. *J. Am. Chem. Soc.* 2009, *131* (22), 7480–7481.

(42) Yang, D.; Xia, L.; Zhao, H.; Hu, X.; Liu, Y.; Li, J.; Wan, X. Preparation and Characterization of an Ultrathin Carbon Shell Coating a Silver Core for Shell-Isolated Nanoparticle-Enhanced Raman Spectroscopy. *Chem. Commun.* 2011, *47* (20), 5873–5875.

(43) Li, D.; Wu, S.; Wang, Q.; Wu, Y.; Peng, W.; Pan, L. Ag@C Core-Shell Colloidal Nanoparticles Prepared by the Hydrothermal Route and the Low Temperature Heating-Stirring Method and Their Application in Surface Enhanced Raman Scattering. *J. Phys. Chem. C* 2012, *116* (22), 12283–12294.

(44) Liu, T.-M.; Yu, J.; Chang, C. A.; Chiou, A.; Chiang, H. K.; Chuang, Y.-C.; Wu, C.-H.; Hsu, C.-H.; Chen, P.-A.; Huang, C.-C. One-Step Shell Polymerization of Inorganic Nanoparticles and Their Applications in SERS/nonlinear Optical Imaging, Drug Delivery and Catalysis. *Sci. Rep.* 2015, *4* (1), 5593.

(45) Mie, G. Beitrage Zur Optik Truber Medien, Speziell Kolloidaler Metallosungen. *Ann. Phys.* 1908, *330* (3), 377–445.

(46) Bohren, C. F.; Huffman, D. R. *Absorption and Scattering of Light by Small Particles*; Bohren, C. F., Huffman, D. R., Eds.; Wiley-VCH Verlag GmbH: Weinheim, Germany, 1998.

(47) Adleman, J. R. Plasmonic Nanoparticles for Optofluidic Applications. Ph.D Thesis, California Institute for Technology, California, USA, 2009.

(48) Kim, Y.; Johnson, R. C.; Li, J.; Hupp, J. T.; Schatz, G. C. Synthesis, Linear Extinction, and Preliminary Resonant Hyper-Rayleigh Scattering Studies of Gold-Core/silver-Shell Nanoparticles: Comparisons of Theory and Experiment. *Chem. Phys. Lett.* 2002, 352 (5–6), 421–428.

(49) Mulvaney, P. Surface Plasmon Spectroscopy of Nanosized Metal Particles. *Langmuir* 1996, 12 (3), 788–800.

(50) Gonçalves, M. R. Plasmonic Nanoparticles: Fabrication, Simulation and Experiments. *J. Phys. D. Appl. Phys.* 2014, 47 (21), 213001.

(51) Bastús, N. G.; Merkoçi, F.; Piella, J.; Puntès, V. Synthesis of Highly Monodisperse Citrate-Stabilized Silver Nanoparticles of up to 200 Nm: Kinetic Control and Catalytic Properties. *Chem. Mater.* 2014, 26 (9), 2836–2846.

(52) Johnson, P. B.; Christy, R. W. Optical Constants of the Noble Metals. *Phys. Rev. B* 1972, 6 (12), 4370–4379.

(53) Palik, E. D.; Ghosh, G. *Handbook of Optical Constants of Solids*; Palik, E. D., Ed.; Academic Press, 1998; Vol. 3.

(54) Ripken, K. Die Optischen Konstanten von Au, Ag Und Ihren Legierungen Im Energiebereich 2,4 Bis 4,4 eV. *Zeitschrift für Phys. A Hadron. Nucl.* 1972, 250 (3), 228–234.

(55) Segelstein, D. J. The Complex Refractive Index of Water. Masters Thesis, University of Missouri Kansas City, Missouri, USA, 1981.

(56) Kyung, K.-H.; Fujimoto, K.; Shiratori, S. Control of Structure and Film Thickness Using Spray Layer-by-Layer Method: Application to Double-Layer Anti-Reflection Film. *Jpn. J. Appl. Phys.* 2011, *50*, 35803.

(57) Haiss, W.; Thanh, N. T. K.; Aveyard, J.; Fernig, D. G. Determination of Size and Concentration of Gold Nanoparticles from UV–Vis Spectra. *Anal. Chem.* 2007, *79* (11), 4215–4221.

(58) Fang, Y.; Seong, N.-H.; Dlott, D. D. Measurement of the Distribution of Site Enhancements in Surface-Enhanced Raman Scattering. *Science* (80-.). 2008, *321* (5887), 388–392.

(59) Tian, J.-H.; Liu, B.; Li; Yang, Z.-L.; Ren, B.; Wu, S.-T.; Tao; Tian, Z.-Q. Study of Molecular Junctions with a Combined Surface-Enhanced Raman and Mechanically Controllable Break Junction Method. *J. Am. Chem. Soc.* 2006, *128* (46), 14748–14749.

(60) *Surface-Enhanced Raman Scattering*; Kneipp, K., Moskovits, M., Kneipp, H., Eds.; Topics in Applied Physics; Springer Berlin Heidelberg, 2006; Vol. 103.

Graphical Abstract

